Nano World Journal

https://doi.org/10.17756/nwj.2023-s3-115

Research Article

Open Access

Thermal Analysis of Low Carbon Steel (SA516 Gr. 70) Welding Through APDL

Mohamed Fayas Saffiudeen* **and Mohammad Nizamuddin Inamdar**

Faculty of Engineering and Built Environment, Lincoln University College, Malaysia

***Correspondence to:**
Mohamed Fayas Saffiudeen
Faculty of Engineering and Built Environment,
Lincoln University College,
Malaysia.
E-mail: mfsaffiudeen@lincoln.edu.my

Received: July 28, 2023
Accepted: October 26, 2023
Published: October 30, 2023

Citation: Saffiudeen MF, Inamdar MN. 2023. Thermal Analysis of Low Carbon Steel (SA516 Gr. 70) Welding Through APDL. *NanoWorld J* 9(S3): S629-S632.

Copyright: © 2023 Saffiudeen and Inamdar. This is an Open Access article distributed under the terms of the Creative Commons Attribution 4.0 International License (CCBY) (http://creativecommons.org/licenses/by/4.0/) which permits commercial use, including reproduction, adaptation, and distribution of the article provided the original author and source are credited.

Published by United Scientific Group

Abstract

The amount of heat that is generated between the shoulder and the work piece is one of the factors that determines the quality of the treated zone that is produced by friction stir processing (FSP). In light of this, having an awareness of the dispersion of heat and acquiring the temperature contours would be helpful in gaining an overall comprehension of the FSP technique. When running the friction stir welding (FSW) simulation, the rotational speed of the tool is either set to 320 or 400 rpm, and both of these speeds allow for some slippage between the shoulder and the work piece. The results of the computational research indicate that the temperature field that is present when the FSW process is being carried out is dispersed in a manner that is symmetrical with regard to the welding line. The primary objective of this study is to conduct research on the temperature shift that takes place on the plate's surface as well as in the heat affected zone after FSW has been performed on a plate composed of SA516 Gr. 70 steel. When it comes to thermal modelling of processes, boundary conditions are an essential component in establishing the overall temperature profile of the system. According to the findings of the virtual experiments that were carried out for the purpose of this study, it was discovered that the peak temperatures reached during the welding process were significantly higher on the advancing side of the joint than they were on the retreating side.

Keywords

Friction stir welding, Low carbon steel, ANSYS, Heat transfer

Introduction

FSP, an offshoot of FSW, has gained significant traction for generating surface layers of metal matrix composites by embedding reinforcement particles onto metal surfaces [1]. An innovative approach involves synergizing FSP and FSW techniques to fabricate FSW joints featuring reinforced nugget zones, wherein researchers have incorporated nano/micro-particles into the adjacent base metals during the FSW operation. However, the integration of nanoparticles into dissimilar FSW remains largely unexplored. In a recent study, Tabasi et al. [2] utilized silicon carbude nanoparticles to conduct dissimilar FSW between AZ31 magnesium alloy and 7075 aluminum alloy, resulting in the formation of a metal matrix composite within the weld stir zone. Following a similar methodology, Pantelis et al. [3] applied the FSW method to introduce silicon carbide nanoparticles into the stir zone during the dissimilar joining process of AA5083 and AA6082 alloys.

Additionally, it's worth noting that the incorporation of nanoparticles into dissimilar FSW presents a novel avenue for enhancing the mechanical and physical properties of welded joints, particularly in terms of strength, hardness, and wear resistance [4, 5]. This innovative approach holds promise for various indus-

trial applications where lightweight, high-strength materials are in demand, such as in aerospace, automotive, and marine engineering [6]. Furthermore, the exploration of different types of nanoparticles, their dispersion methods, and their effects on the microstructure and performance of dissimilar friction stir welded joints opens up avenues for further research and optimization in the field of advanced materials joining [7, 8].

As a promising way to enhance joint properties by making composite joints, nanomaterial reinforced FSW is an emerging area. A composite joint can improve surface properties such as hardness, strength, corrosion resistance, wear resistance, fatigue life, and electrical conductivity [9]. As a reinforcement agent for FSW, nanoparticles are currently being used by researchers. Among the reinforcement materials used in FSW are copper metal nanoparticles, titanium dioxide nanoparticles, titanium carbide nanoparticles, etc. Because of their exceptional mechanical, chemical, thermal, and tribological properties, carbonaceous nanomaterials, including carbon nanotubes and graphene, are gaining interest as potential reinforcing nanomaterials for FSW [9].

In composites, nanoceramic reinforcement is extensively used due to its excellent properties at simple structures. In addition to enhanced mechanical properties (such as tensile strength, fatigue strength, and hardness), nano reinforced composites have high thermal stability, as well as better chemical and tribological properties [10]. Because of their exceptional physical, mechanical, electrical, and thermal characteristics, carbon nanotubes and graphene have emerged as ideal reinforcement for composite structures. Based on these excellent properties, a study was conducted to make composites with FSW [11].

Experimentation

An examination of the relevant literature indicated that shielded metal arc welding, gas tungsten arc welding, and laser welding are all viable industrial welding procedures for low carbon steel. Another approach that was determined to be viable was FSW (Figure 1). On the other hand, there is an extreme lack of published data about FSW of HSLA SA516 grade 70 steel (Table 1 and table 2). The primary objective of the ongoing research is to develop a method for the autogenous welding of SA516 grade 70 steel using submerged FSW. The relationship between spindle speed and welding speed was investigated, specifically with regard to the minimum bead width and maximum penetration depth. In addition, the mechanical and metallurgical properties of the weldment were investigated. Weld joints made of SA516 steel that are utilized in power plants stand to gain a great deal from the findings of this study.

There is a paucity of published research on the topic of optimizing FSW by adjusting the welding parameters (Rotation speed (N), tool traverse speed (v), sxial (plunging) force (F_z), and plunge depth) in relation to the ASME SA516 Gr. 70 weld bead geometry properties (Table 3). This is due to the fact that very few studies have been conducted on this topic. Because FSW of this grade steel is so commonly used in the pressure vessel sector, it is essential to have a solid understanding of how the various process factors influence the quality of the weld.

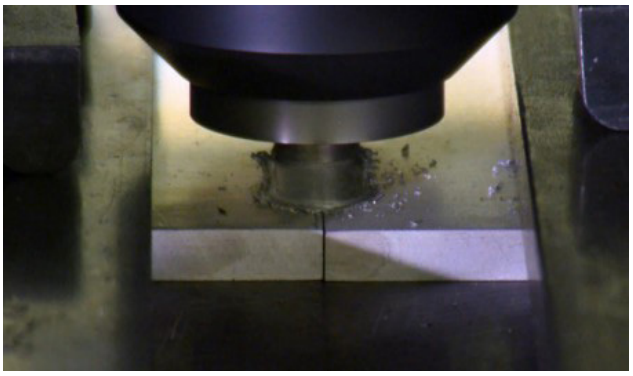

Figure 1: FSW.

Table 1: Chemical composition of SA516 grade 70 steel.

Element	Observed values
C	0.222
Si	0.320
Mn	1.12
P	0013
S	0.007
Cr	0.048
Mo	0.006
Ni	0.012
Cu	0.018
Nb	0.014
Ti	0.002
V	0.005
B	0.001
N	0.006

Table 2: Mechanical properties - SA516 grade 70 steel.

Yield strength, MPa	340 - 345
Ultimate tensile strength, MPa	562 - 565
% of elongation	31 - 35
Impact energy, J	5.51 - 5.55

Table 3: Process parameters of FSW.

FSW parameter	Range of values
Rotation speed (N)	320 - 5500 rpm
Tool traverse speed (v)	25 - 455 mm/min
Axial (plunging) force (F_z)	210 - 11,500 N
Plunge dep	0.1 - 0.4 mm

The current analysis makes use of fine FEA mesh, which may result in outputs that are practically exactly the same; nevertheless, the amount of time spent calculating rose significantly. For the purpose of carrying out transient thermal assessments, a piece of software called as APDL (ANSYS Parametric Design Language) was developed. In order to de-

termine the temperature distribution that takes place within the welded steel plates while the welding process is taking place, calculations are carried out making use of transient thermal finite elements. The temperature profiles that were present in the workpiece are depicted in figure 2 and figure 3, respectively, when welding operations were being carried out at speeds of 3 m/s and 500 rpm, respectively. When a load is applied, all of the energy that is lost due to friction is turned into heat. This happens whenever the load is applied. Heat is produced whenever the tool and the workpiece are in close proximity to one another and come into touch with one another. The object that is being worked on takes up the vast bulk of the heat that is generated.

Results and Discussion

Temperature distribution

The temperature of the work piece rises at a pace that is significantly faster than the temperature of the tool. Compare and contrast these two rates. If the heat input from the pin is disregarded, it will not be feasible to accurately portray the heat transfer process over the whole of the tool penetration period.

When attempting to estimate the preheat effects of laser assisted preheated FSW, it is of the utmost importance to have an accurate representation of the initial field in a model of transient heat transfer. Because of this, it is extremely important for heat transfer to occur during the phase in which the tool is piercing the material, as this is the phase in which it is most likely to occur. The nugget's calculated peak temperature is approximately 590 degrees Celsius when rotating at 250 rpm; the TMAZ's calculated peak temperature is between 481 and 512 degrees Celsius; and the heat affected zone calculated peak temperature is between 512 and 449 degrees Celsius. Figure 4 and figure 5 show, respectively, the temperature distribution in ASME SA516 Gr. 70 steel that was welded at 400 and 320 rpm. It indicates that there will be a rise in temperature even if there is no change in the tool speed at all.

Temperature gradient

Simulations of heat transmission were performed with the steel graded as ASME SA516 Gr. 70 in this particular instance. In this particular area, just the most recent or most recent of all possible numerical results are offered. The FSW process generates heat, which along with the friction, quickly spreads to areas of the plates that were previously inaccessible. Heat is lost to the environment around the work item as a result of convection and radiation from the top and side surfaces of the work item. Conduction losses can also be detected stretching from the bottom surface of the work piece all the way to the backing plate. This can be seen as a negative effect of the material. It is estimated that the convection coefficient for the workpiece surfaces, with the exception of the bottom surface, will range from 10 to 30 W/m^{2}°C. The bottom surface will have a convection value of 0. Both the workpiece and the tool have a convection coefficient of 30 W/m^{2}°C when it comes to temperature.

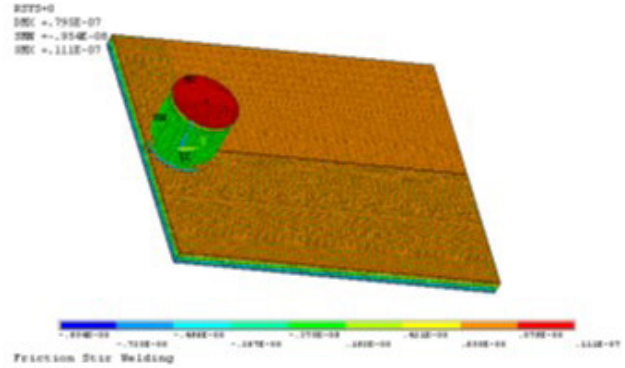

Figure 2: Load step 1 at 400 rpm.

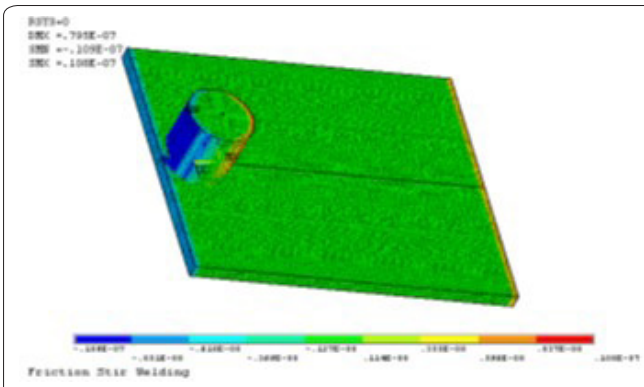

Figure 3: Load step 1 at 320 rpm.

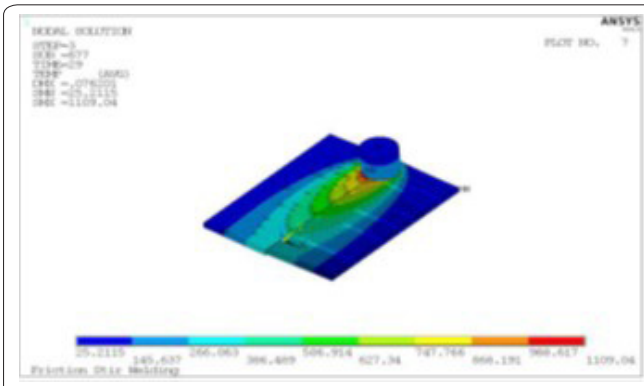

Figure 4: Temperature distribution at 400 rpm.

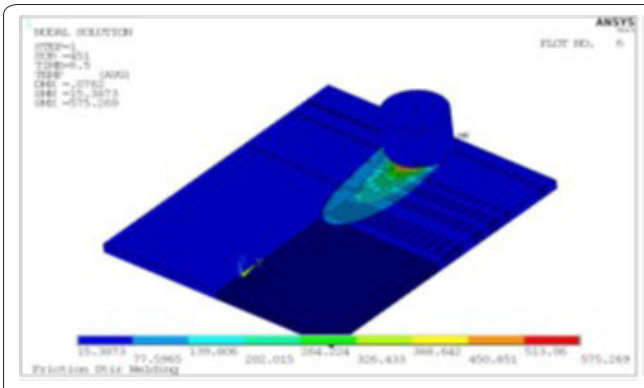

Figure 5: Temperature distribution at 320 rpm.

The temperature of the output is in part determined by the effect that this coefficient plays. When a lesser coefficient is utilised, the model generates a higher temperature as an output. When there is a high overall heat-transfer coefficient, such as 280 W/m^{2}°C, it is reasonable to assume that the bottom surface of the workpiece will suffer heat loss as a result of conduction. It is required to consider the bottom surface of the workpiece to be a convection surface in order to model the losses that occur due to conduction. This is because the conduction losses are simulated using a computer. Heat loss that is caused by radiation is not taken into account because there is only a little amount of it. The temperature of the model will start out at 25 degrees Celsius when it is first run. There is not the slightest indication that temperature boundary constraints are being implemented in any way, shape, or form anywhere in the model [12, 13].

Conclusions

When the results of the experiments that were relevant to the contact circumstances are analysed, one can glean insightful information regarding the progression of the relative sliding that takes place between the shoulder and the material that is going to be welded. This information can be obtained by looking at the results of the experiments. In addition to that, the results of this study allow for accurate forecasting of the temperature distribution in a variety of distinct zones in relation to a number of various parameters.

- The data obtained from the virtual tests reveal that the temperature of the weldment rises when the rotational speed of the tool is increased, but that the temperature of the weldment falls when the welding speed is increased. In contrast to this, the circumstance in which the temperature of the weldment rises while the welding speed falls does not occur. In addition, the finding appears to suggest that the temperature on the front of the vehicle is higher than the temperature on the back of the vehicle at the same time.
- Because this task involves a moving coordinate, there are no moving heat sources; as a result, the model can be easily applied to the heat-transfer process that takes place during FSW for both the tool and the workpiece. This is because heat is transferred from the tool to the workpiece at the same rate as it is transferred from the tool to the workpiece.
- The findings of the computational analysis demonstrate that there is an asymmetry of the temperature profiles around the tool as a result of the rotational and linear motion of the tool, as well as an asymmetry of the heat generation around the tool pin surface. This asymmetry can be attributed to the fact that the rotational and linear motion of the tool causes the tool to move in different directions. This asymmetry can be explained by the fact that the tool moves in separate directions as a result of its rotational motion and linear motion (both of which cause the tool to move).

Acknowledgements

None.

Conflict of Interest

None.

References

1. Barmouz M, Asadi P, Givi MB, Taherishargh M. 2011. Investigation of mechanical properties of Cu/SiC composite fabricated by FSP: effect of SiC particles' size and volume fraction. *Mater Sci Eng A* 528(3): 1740-1749. https://doi.org/10.1016/j.msea.2010.11.006
2. Tabasi M, Farahani M, Givi MB, Farzami M, Moharami A. 2016. Dissimilar friction stir welding of 7075 aluminum alloy to AZ31 magnesium alloy using SiC nanoparticles. *Int J Adv Manuf Technol* 86: 705-715. https://doi.org/10.1007/s00170-015-8211-y
3. Pantelis DI, Karakizis PN, Daniolos NM, Charitidis CA, Koumoulos EP, et al. 2016. Microstructural study and mechanical properties of dissimilar friction stir welded AA5083-H111 and AA6082-T6 reinforced with SiC nanoparticles. *Mater Manuf Process* 31(3): 264-274. https://doi.org/10.1080/10426914.2015.1019095
4. Alidokht SA, Abdollah-Zadeh A, Soleymani S, Assadi H. 2011. Microstructure and tribological performance of an aluminium alloy based hybrid composite produced by friction stir processing. *Mater Des* 32(5): 2727-2733. https://doi.org/10.1016/j.matdes.2011.01.021
5. Hamdollahzadeh A, Bahrami M, Nikoo MF, Yusefi A, Givi MB, et al. 2015. Microstructure evolutions and mechanical properties of nano-SiC-fortified AA7075 friction stir weldment: the role of second pass processing. *J Manuf Process* 20: 367-373. https://doi.org/10.1016/j.jmapro.2015.06.017
6. Nikoo MF, Azizi H, Parvin N, Naghibi HY. 2016. The influence of heat treatment on microstructure and wear properties of friction stir welded AA6061-T6/Al_2O_3 nanocomposite joint at four different traveling speed. *J Manuf Process* 22: 90-98. https://doi.org/10.1016/j.jmapro.2016.01.003
7. Dragatogiannis DA, Koumoulos EP, Kartsonakis IA, Pantelis DI, Karakizis PN, et al. 2016. Dissimilar friction stir welding between 5083 and 6082 Al alloys reinforced with TiC nanoparticles. *Mater Manuf Process* 31(16): 2101-2114. https://doi.org/10.1080/10426914.2015.1103856
8. Abdollahzadeh A, Shokuhfar A, Omidvar H, Cabrera JM, Solonin A, et al. 2019. Structural evaluation and mechanical properties of AZ31/SiC nano-composite produced by friction stir welding process at various welding speeds. *Proc Inst Mech Eng Part L J Mater Des Appl* 233(5): 831-841. https://doi.org/10.1177/1464420717708485
9. Raja S, Muhamad MR, Jamaludin MF, Yusof F. 2020. A review on nanomaterials reinforcement in friction stir welding. *J Mater Res Technol* 9(6): 16459-16487. https://doi.org/10.1016/j.jmrt.2020.11.072
10. Maitra S, Roy J. 2018. Nanoceramic Matrix Composites: Types, Processing, and Applications. In Low IM (ed) Advances in Ceramic Matrix Composites. Woodhead Publishing.
11. Baig Z, Mamat O, Mustapha M. 2018. Recent progress on the dispersion and the strengthening effect of carbon nanotubes and graphene-reinforced metal nanocomposites: a review. *Crit Rev Solid State Mater Sci* 43(1): 1-46. https://doi.org/10.1080/10408436.2016.1243089
12. Kumar P, Sinha AN. 2018. Studies of temperature distribution for laser welding of dissimilar thin sheets through finite element method. *J Braz Soc Mech Sci Eng* 40(9): 455. https://doi.org/10.1007/s40430-018-1380-5
13. Sagar P, Gope DK, Chattopadhyaya S. 2018. Thermal analysis of TIG welded Ti-6Al-4V plates using ANSYS. *IOP Conf Ser Mater Sci Eng* 377(1): 012113. https://doi.org/10.1088/1757-899X/377/1/012113